Article

Polyarylamine-Based Polymeric Electret with Tunable Pendant Groups for Photorecoverable Organic Transistor Memory

Bo-Yuan Chuang,[||] Chun-Yao Ke,[||] Yu-Jen Shao,[||] Ken-Tsung Wong,* and Guey-Sheng Liou*

Read Online

ACCESS | Metrics & More | Article Recommendations | Supporting Information

ABSTRACT: Polyarylamine-based dielectric electrets and pentacene as p-type semiconductors have been utilized to fabricate photoresponsive flash transistor memories. In this study, three polyarylamines, **PTTC** (poly(5-(4-(diphenylamino)phenyl)-thiophene-2-carbonitrile)), **PTTP** (poly(N,N-diphenyl-4-(5-phenylthiophen-2-yl)aniline)), and **PDTPmC** (poly(2-(5-(diphenylamino)thiophen-2-yl)pyrimidine-5-carbonitrile)), with different pendant moieties, have been synthesized and characterized. They have been investigated for their ability to trap holes and photorecovery behaviors. The **PDTPmC** electret, which features a high dipole moment, coplanar conformation, and highly conjugated structure, has demonstrated an outstanding hole-trapping capability with a memory window of 106 V and photorecoverability under light irradiation. The coplanar donor−acceptor configuration converging diphenylamine and thiophene-pyrimidine provides sufficient hole-trapping sites and delocalization ability for photoexcitation excitons. The **PDTPmC**-based memory device exhibits excellent switching reliability of electrical programming and optical erasing for 200 cycles, with a stable readout current ratio of approximately 10^5. This study proposes a polymer electret design approach to achieve high-performance transistor memory and photorecording device characteristics.

KEYWORDS: polymer electret, triphenylamine, conjugated polymer, photoinduced recovery, transistor memory
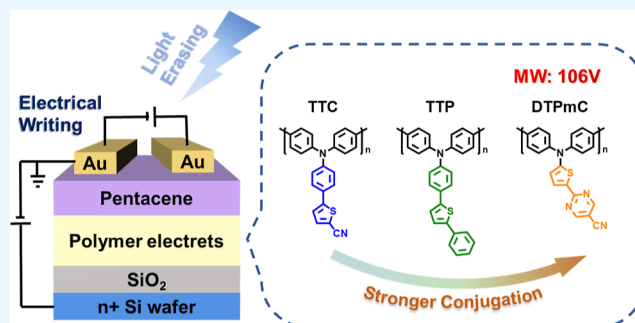
1. INTRODUCTION

The demand for ultrahigh-density charge storage has dramatically increased with the advancement of artificial intelligence (AI) and the Internet of Things (IoT). The efficiency improvement of traditional inorganic memory devices has gradually failed to keep up.[1] Organic memory devices are emerging as a research direction due to their low cost, lightweight,[2] and ability to tune the charge storage properties of organic materials through careful molecular design. Among the various configurations of organic memory devices, field-effect transistor (FET)-type devices are characterized by the nondestructive readout, compatibility with circuit integration, and the ability to store multiple bits in a single working unit.[3] The configuration of organic field-effect transistor memory (OFETM) devices is similar to that of ordinary FETs but with an additional charge storage layer between the semiconductor and dielectric layers. The currently studied charge storage materials mainly include ferroelectric materials,[4] nanofloating gate dielectric materials,[5] and polymer electrets.[6] Among them, polymeric electrets are advantageous because they can achieve high storage efficiencies without the need for costly inorganic nanoparticles or limiting the selection to ferroelectric materials. The polymer design will primarily affect the charge storage capacity, manifested by the readout current on/off ratio and memory window.[7] For example, Hsu

et al. found that the memory windows could be enlarged by increasing the conjugation length of the pendent side chains.[8] Nevertheless, for conventional electrical-driven OFETM devices, the energy consumption in writing and erasing (ERS) information is significantly large.[9] Recently, an optical-driven process could partially[10−12] or wholly replace the electrical-driven operation,[13] reducing energy consumption considerably. Furthermore, the interference between the two orthogonal driving operations will be much lower in a half-light-driven, half-electrical-driven transistor memory device.

Photoresponsive polymers with an appropriate absorption band can absorb light to generate excitons that are helpful for the trapped charges to be recombined and transferred back to the semiconductor layer.[14−17] For example, a carbazole-dioxazine-based polymer (Poly CD) as a charge storage material for photorecoverable OFET memory devices was recently reported. The storage window reaches 82 V under a negative voltage pulse of −90 V.[18] Compared to polyether-
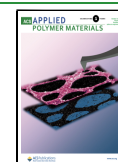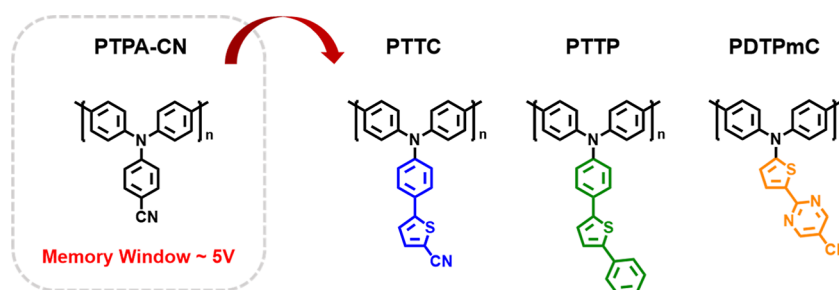
Figure 1. Chemical structures of **PTTC**, **PTTP**, **PDTPmC**, and reported **PTPA-CN**.

based polymeric electrets, conjugated-based polymeric electrets with a facile synthetic method and highly tunable structures efficiently satisfy the required demand, including photoresponse ability, intramolecular dipole moment, energy level, etc. Therefore, in our previous work, the poly-(triphenylamine)-based donor–acceptor-type conjugated polymers are photoresponsive material that can be used as a charge storage electret in photorecoverable OFET memory devices.[19] The memory window of PTPA-CN-based devices is only 5 V, even under a negative voltage pulse of −120 V, in addition to the incapability to capture high charge densities. While the PTPA-CNBr demonstrated enhanced memory performance compared to PTPA-CN, mainly due to its increased hole-trapping capability resulting from the extension of conjugation length. Nevertheless, modifying the chemical structures of PTPA-CNBr to improve the charge coplanarity is not easy.[33–35] Hence, in this study, to enhance the performance of PTPA-CN, we report the design and synthesis of three diphenyl-amine-based polymers, **PTTP**, **PTTC**, and **PDTPmC** (Figure 1), via the oxidative coupling reaction with FeCl₃ as an oxidative agent. Thiophene was introduced as a π-linker to the pendant conjugated side chain of **PTPA-CN** to obtain **PTTC**, which would be expected to increase the memory window, because of the extended conjugation length. On the other hand, the cyano group of **PTTC** was replaced by the phenylene ring for **PTTP**, designed as the non-D–A counterpart of **PTTC**. The relatively longer conjugation length of the pendant may lead to a higher charge storage capacity. In addition, *N,N*-diphenylthiophen-2-amine was used as the donor unit of the polymer **PDTPmC** to reduce the steric hindrance and enhance the electron-donating strength. Due to the less steric effect, the conformation of the thiophene-pyrimidine linkage in **DTPmC** is more coplanar. In addition, the donor–acceptor–acceptor (D–A–A) configuration of **DTPmC** leads to an enhanced intramolecular charge transfer (ICT). These two properties may result in stronger pendant side chain conjugation than the other two polymers, strengthening the charge storage ability.

Furthermore, the light-induced recovery of the stored charges was investigated by utilizing these polymers as electret layers. All three polymers exhibit matched energy levels, allowing negative-voltage-driven hole transfer and trapping holes from the pentacene layer. Then, the accumulated charges are photorecoverable. We found that the hole-trapping ability of the polymeric electrets positively correlated with the conjugation ability of the pendant side chain. Among them, **PDTPmC** electret featuring the longest side-chain conjugation achieves a memory window of 106 V due to the strong ICT effect and high coplanarity, which is particularly remarkable in terms of memory efficiency among previous studies.

2. EXPERIMENTAL SECTION

2.1. Materials. All chemicals were purchased from commercial sources and used as received without purification. The precursors 4-(5-bromothiophen-2-yl)-N,N-diphenylamine (**1**) and 5-(5-bromopyr-imidin-2-yl)-*N,N*-diphenylthiophen-2-amine (**2**) were synthesized according to the previous literature.[20,21]

2.2. Synthetic of Monomer. *2.2.1. N,N-Diphenyl-4-(5-phenyl-thiophen-2-yl)aniline (TTP).* A mixture of **1** (1.00 g, 2.46 mmol), phenylboronic acid (0.36 g, 2.95 mmol), palladium-tetrakis-(triphenylphosphine) (57 mg, 0.049 mmol), and potassium carbonate (1.00 g, 7.38 mmol) in a solvent mixture of dry toluene (13 mL), ethanol (3 mL), and distilled water (3 mL) was heated at 100 °C and stirred for 17 h under an argon atmosphere. After cooling to room temperature, the solvent was removed by rotary evaporation, and the reaction mixture was then extracted with dichloromethane (DCM). The combined extracts were washed with brine, dried over anhydrous magnesium sulfate, and filtered. After the crude product was concentrated by rotary evaporation, it was purified by silica gel column chromatography using CH_2Cl_2/hexane (v/v, 2:1) as the eluent to obtain the yellow crystal **TTP** (0.50 g, 1.23 mmol, 50%). mp 141−144 °C¹H NMR (CDCl₃, 400 MHz, δ) 7.63 (d, J = 7.5 Hz, 2H), 7.50 (d, J = 8.8 Hz, 2H), 7.38 (t, J = 7.5 Hz, 2H), 7.31−7.24 (m, 7H), 7.21 (s, 1H), 7.13 (d, J = 7.5 Hz, 4H), 7.08 (d, J = 8.8 Hz, 2H), 7.04 (d, J = 7.5 Hz, 2H). ¹³C NMR (CDCl₃, 100 MHz, δ): 147.44, 147.26, 143.50, 142.66, 134.36, 129.30, 128.87, 128.33, 127.31, 126.38, 125.48, 124.49, 123.96, 123.64, 123.08. MALDI-MS: found *m/z* 403.1375; calculated for $[M^+]$ 403.14. Elemental Anal. Calcd for $C_{28}H_{21}NS$: C, 83.34; H, 5.25; N, 3.47, Found: C, 83.25; H, 4.86; N, 3.48.

2.2.2. 5-(4-(diphenylamino)phenyl)thiophene-2-carbonitrile (TTC). A mixture of **1** (2.57 g, 6.32 mmol), zinc cyanide (0.88 g, 7.60 mmol), and palladium-tetrakis(triphenylphosphine) (1.09 g, 0.948 mmol) in dry DMF (62 mL) was heated at 100 °C and stirred for 17 h under an argon atmosphere. After cooling to room temperature, the solvent was removed by rotary evaporation, and the reaction mixture was then extracted with ethyl acetate (EA). The combined extracts were washed with brine, dried over anhydrous magnesium sulfate, and filtered. After the crude product was concentrated by rotary evaporation, it was purified by silica gel column chromatography using CH_2Cl_2/hexane (v/v, 2:1) as the eluent to obtain the light green crystal **TTC** (1.00 g, 2.84 mmol, 45%). mp 138−141 °C, ¹H NMR (CDCl₃, 400 MHz, δ) 7.55 (d, J = 3.6 Hz, 1H), 7.43 (d, J = 8.8 Hz, 2H), 7.31−7.27 (m, 4H), 7.17−7.04 (m, 9H). ¹³C NMR (CDCl₃, 100 MHz, δ): 151.88, 149.02, 146.88, 138.43, 129.44, 127.13, 125.32, 125.08, 123.83, 122.40, 121.94, 114.62, 106.72. MALDI-MS: found *m/z* 352.1016; calculated for $[M^+]$ 352.10. Elemental Anal. Calcd for $C_{23}H_{16}N_2S$: C, 78.38; H, 4.58; N, 7.95, Found: C, 77.70; H, 4.46; N, 7.86.

2.2.3. 2-(5-(diphenylamino)thiophen-2-yl)pyrimidine-5-carbon-itrile (DTPmC). A mixture of **2** (1.80 g, 4.41 mmol), zinc cyanide (632 mg, 5.29 mmol), palladium-tetrakis(triphenylphosphine) (510 mg, 0.441 mmol), and tri*tert*-butylphosphonium tetrafluoroborate (256 mg, 0.882 mmol) in dry DMF (44 mL) was heated to 100 °C and stirred for 2 h under an argon atmosphere. After cooling to room temperature, the solvent was removed by rotary evaporation, and the reaction mixture was then extracted with ethyl acetate (EA). The
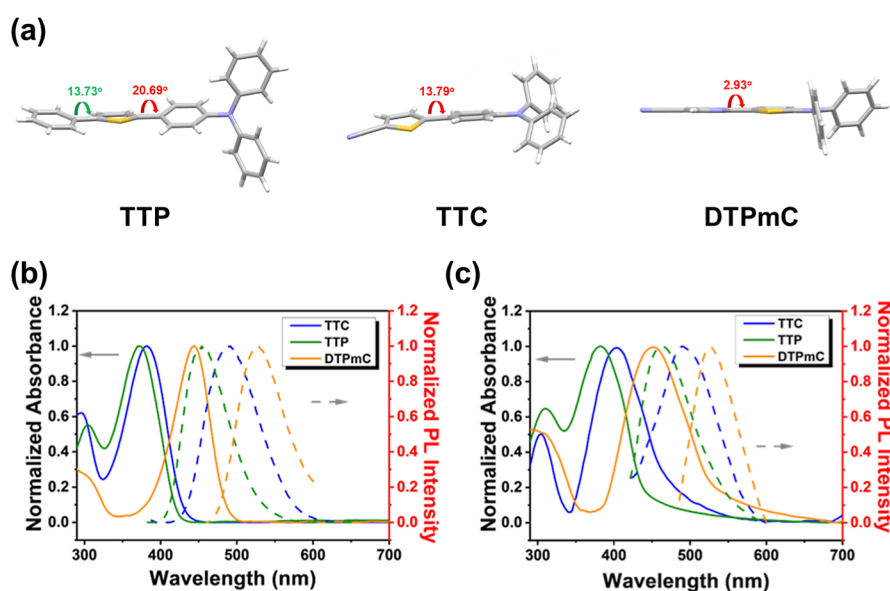
Figure 2. (a) Single crystal geometry of **TTC**, **TTP**, and **DTPmC**, respectively. (b,c) Normalized UV−vis absorption and PL spectra of **TTC**, **TTP**, and **DTPmC** in (b) DCM solution and (c) solid state.

combined extracts were washed with brine, dried over anhydrous magnesium sulfate, and filtered. After the crude product was concentrated by rotary evaporation, it was purified by silica gel column chromatography using CH_2Cl_2/hexane (v/v, 2:1) as the eluent to obtain orange crystal **DTPmC** (1.36 g, 3.84 mmol, 87%). mp 151−154 °C, ^1H NMR (CDCl$_3$, 400 MHz, δ) 8.70 (s, 2H), 7.87 (d, J = 4.4 Hz, 1H), 7.39−7.31 (m, 5H), 7.29 (d, J = 8.8 Hz, 5H), 7.22−7.15 (m, 2H), 6.49 (d, J = 4.4 Hz, 1H). ^{13}C NMR (CDCl$_3$, 100 MHz, δ): 162.42, 161.94, 159.39, 146.36, 133.39, 129.71, 127.98, 125.57, 125.12, 115.64, 114.72, 103.14. MALDI-MS: found m/z 354.0918; calculated for $[M^+]$ 354.09. Elemental Anal. Calcd for $C_{21}H_{14}N_4S$: C, 71.17; H, 3.98; N, 15.81, Found: C, 71.29; H, 3.88; N, 15.93.

2.3. Preparation of the Polyarylamines via Oxidative Polymerization. Take **TTC** as an example of the general synthetic route. In a two-necked 50 mL flask covered with aluminum foil to avoid light exposure and equipped with a condenser after **TTC** (1 mmol) was dissolved in o-DCB (20 mL) and heated to 70 °C under a nitrogen atmosphere, FeCl$_3$ (4 mmol, 1 mmol each) was added four portions in sequence into the mixture at the interval of 1 h. After reacting for 24 h, the mixture was poured into methanol with 10% hydrochloric acid to precipitate, collected by filtration, and washed in methanol/NH$_4$OH overnight. After drying in vacuum at 75 °C, the crude product was dissolved in chloroform and filtrated to separate the nondissolved part. Then, the filtrate was reprecipitated in the methanol solution and underwent the Soxhlet extraction with methanol. The final product was dried at 100 °C in vacuum overnight (yield: 63%).

3. RESULTS AND DISCUSSION

3.1. Synthesis and Characterization of Monomer. The syntheses and chemical structures of the monomers are depicted in Scheme S1. Following the literature procedures, triarylamine derivatives 1 and 2 were synthesized using the Suzuki and Negishi coupling reactions.[20,21] The nitrile-substituted molecules, **TTC** and **DTPmC**, were prepared by palladium-catalyzed cyanation using zinc cyanide as the cyanide source. **TTP** was obtained by Suzuki coupling of **1** with phenylboronic acid. The obtained monomers **TTP**, **TTC**, and **DTPmC** were characterized in detail by ^1H NMR (Figure S1), FT-IR spectroscopy (Figure S2), mass spectrometry, and elemental analysis. In addition, the crystals suitable for X-ray

analysis were obtained by a liquid−liquid diffusion method using hexane and DCM as a binary solvent system. The single crystals data are summarized in Table S1. As indicated in Figure 2a, introducing thiophene into the pendant groups leads these molecules to have less-twisted conformations between aromatic rings, particularly for **DTPmC**, which reaches an almost coplanar configuration. The molecular conformations benefit the π-conjugation and ICT characters. Figure 2b,c depict **TTP**, **TTC**, and **DTPmC** photophysics in dichloromethane (DCM) solutions and thin films cast from chloroform solutions, respectively. The corresponding data are summarized in Table S2. The absorption maximum ($\lambda_{abs, max}$) of **TTP** is mainly ascribed to the $\pi−\pi^*$ transition of the π-conjugated pendant. By replacing the terminal phenyl group with an electron-withdrawing cyano group, the $\lambda_{abs, max}$ of **TTC** is red-shifted due to the ICT effect. The ICT influence is even more significant in **DTPmC**, resulting in the most red-shifted $\lambda_{abs, max}$ of 444 nm in the DCM solution due to its unique D−A−A-type configuration and high coplanarity (dihedral angle $\approx 2.93°$), causing the most potent ICT effect on the conjugation backbone.[22] In the solid state, **TTP**, **TTC**, and **DTPmC** absorptions are red-shifted compared with those observed in DCM, mainly due to the intermolecular interactions. In addition to the electronic absorption, the photoluminescence (PL) spectra of **TTP**, **TTC**, and **DTPmC** were measured. The PL λ_{max} reveals a shifting tendency similar to the absorption behavior observed in solution and the solid states. The PL of **TTP**, **TTC**, and **DTPmC** manifests a high quantum yield (Φ_{PL}) of 81, 94, and 67%, respectively, in DCM solution. However, all monomers exhibit relatively weak PL behavior in the solid state with a decreased Φ_{PL}. The weak PL in the solid state could attribute to dipole−dipole-induced emission quenching caused by intermolecular interactions in thin films.[23] Among the three monomers, **DTPmC** exhibits the most significantly decreased Φ_{PL}, dropping to 4% in the solid state, owing to the shortest intermolecular $\pi−\pi$ distance (3.69 Å) that results in the strongest aggregation-induced fluorescence quenching (Figures S3−S5).
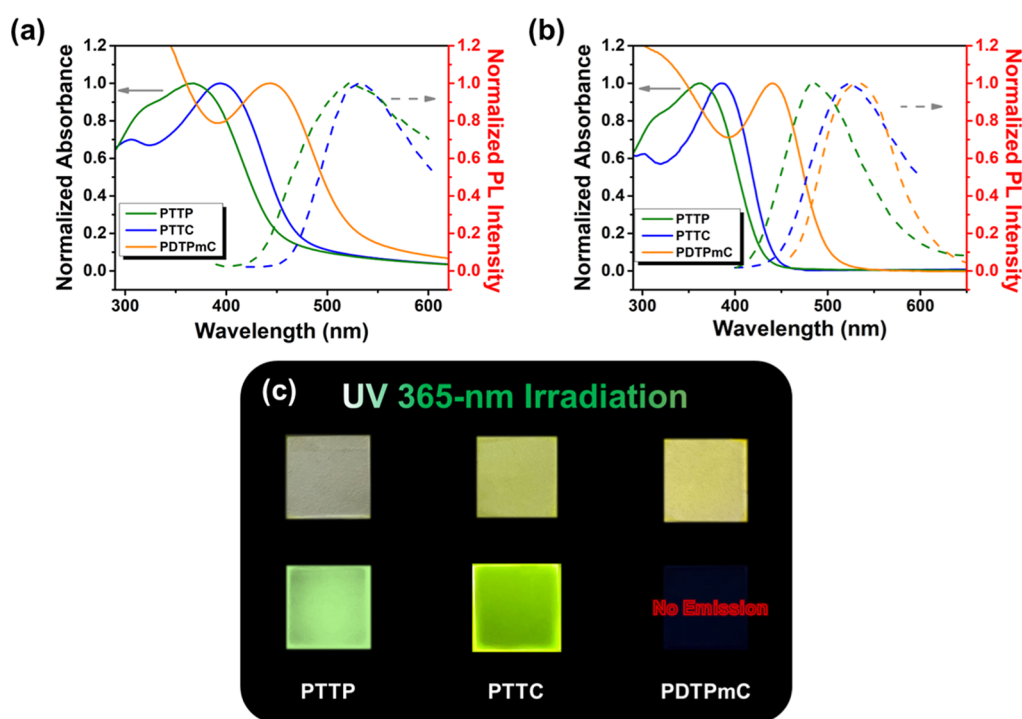
Figure 3. Normalized absorption and photoluminescence spectra of the **PTTC**, **PTTP**, and **PDTPmC** polymers in (a) film state and (b) THF solution (**PDTPmC** is nonemissive in the film state). (c) Photos of the resulting polymer films under (up) room light and (down) 365 nm irradiation.

The electrochemical properties of these compounds were examined by cyclic voltammetry (CV), as depicted in Figure S6, and the results are summarized in Table S3. **TTP** and **TTC** reveal a quasi-reversible oxidation potential at 0.37 and 0.52 V, respectively, relative to the oxidation potential of ferrocene, which can be attributed to the oxidation of triphenylamine. The highest occupied molecular orbital (HOMO) level of **TTC** is estimated to be −5.32 eV, which is lower than that of **TTP** (−5.17 eV) due to the electron-withdrawing nature of the cyano group. On the other hand, **DTPmC** exhibits irreversible oxidation at 0.56 V, indicating less electrochemical stability. The HOMO energy level of **DTPmC** estimated from the onset of the oxidation potential is −5.37 eV due to the compensation effects of the electron-rich thiophene ring and the stronger electron-withdrawing CN-substituted pyrimidine moiety. **DTPmC** exhibits a quasi-reversible reduction potential at 1.85 V. In contrast, the quasi-reversible and irreversible reductions of **TTC** and **TTP** occur at 2.19 and 2.20 V (onset), respectively, indicating that **DTPmC** exhibits a more substantial electron-accepting capability. Using the obtained HOMO levels and optical energy gaps, the lowest unoccupied molecular orbital (LUMO) energy levels of **TTP**, **TTC**, and **DTPmC** are calculated as −2.24, −2.46, and −2.82 eV, respectively.

The HOMO and LUMO energy levels of these monomers are consistent with the trends calculated by DFT at the B3LYP/6-31G (d,p) level (Figure S7). The ground state dipole moments of the monomers **TTP**, **TTC**, and **DTPmC** were also calculated, giving 0.87 7.04, and 7.21 D, respectively. The obtained single crystals of three monomers (Figure 2a) showed that the dihedral angle structure between the phenylene ring and thiophene of **TTC** is 13.8°, while the dihedral angles of the two phenyl rings and thiophene of **TTP** are 13.7 and 20.7°, respectively. As for **DTPmC**, because of the

low steric effect between the thiophene and the pyrimidine, its dihedral angle is only 2.9°, resulting in much more coplanarity than those of **TTC** and **TTP**. The degree of bond length alternation (BLA) shown in Table S4, calculated as the difference between the bond length of C2−C3 and the average bond lengths of C1−C2 and C3−C4 of the thiophene π-linker, is 0.044 Å for **TTC** and 0.036 Å for **TTP**. The C4−C5 bonding distances between the triphenylamine and thiophene unit are 1.466 Å for **TTC** and 1.458 Å for **TTP**. The lower degree of BLA and the shorter C4−C5 bond length of **TTP** imply that **TTP** has a stronger π-electron delocalization than **TTC**, indicating the longer conjugation length of **TTP**. Previous studies have demonstrated that conjugated chains with greater polarity would lead to more charge dissipation.[24] However, when the ICT effect is enhanced, it may also make a larger memory window of the device.[25] This trade-off viewpoint is inspiring and elucidated in subsequent experiments.

3.2. Characterization of Polyarylamines. The polyarylamines, **PTTC**, **PTTP**, and **PDTPmC**, were prepared by oxidative polymerization in the presence of anhydrous FeCl₃ in *o*-DCB at 70 °C for 24 h. The detailed characterizations of the prepared polymers, including IR, NMR, and GPC measurements, are reported in the Supporting Information (Figures S8 and S9 and Table S5). These polymers revealed excellent thermal stability with the T_d^5 (5 wt % weight loss) above 300 °C. Among these polymers, **PDTPmC** exhibits the highest T_g up to 198 °C because of its highly planar structure and rigid polymer backbone, as shown in Figure S10 and Table S6.

After the oxidative polymerization, the PL λ_{max}s of the obtained polyarylamines exhibit more red-shifted characteristics compared to those of the corresponding monomers in both solution and film states, as shown in Figure 3 and Table 1, implying that the polymers with increased chain lengths were

Table 1. Photophysical Properties of the Monomers and the Resulting Polyarylamines in the Solution and Solid States

	THF Solution (10 μM)			solid state		
index	$\lambda_{abs, max}$ [nm]	$\lambda_{em, max}$ [nm]^a	Φ_{PL} [%]^b	$\lambda_{abs, max}$ [nm]	$\lambda_{em, max}$ [nm]^a	Φ_{PL} [%]^b
Monomer						
TTC	382	490	94	404	490	68
TTP	373	454	81	381	463	28
DTPmC	444	526	67	453	526	4
Polymer						
PTTC	385	522	53	407	534	9
PTTP	362	487	48	368	524	2
PDTPmC	430	542	2	443	n.d^c	n.d

$^a\lambda_{em, max}$ was excited at the wavelength of $\lambda_{abs, max}$. $^b\Phi_{PL}$ was calculated by using an integrated sphere. ^{c}Not detectable.

successfully synthesized. Compared to the corresponding highly luminescent monomers, polymers **PTTC** and **PTTP** preserve the intensely luminescent ability in the solution state with Φ_{PL} values of 53 and 48%, respectively. However, the polymer films showed relatively weak luminescence with Φ_{PL} of 9% for **PTTC** and 2% for **PTTP**, indicating that the chain-to-chain energy transfer occurred due to the stacking of the conjugated polymer chains. In contrast, the Φ_{PL} of **PDTPmC** in solution is only 2%. At the same time, the PL of the **PDTPmC** film is completely quenched, which could be attributed to the strong interchain interactions stemming from the highly planar and polar pendant group.

3.3. Electrical Characteristics of P-Type Transistor Memory Devices. Figure 4 illustrates a schematic diagram of a pentacene transistor memory device constructed with polyarylamines (PAAs) electrets coated on top of a silicon dioxide/silicon substrate in a bottom-gate-top-contact configuration. The thickness of building layers was controlled to 40 nm for polymer electrets, 50 nm for the pentacene semiconductor, and 70 nm for gold electrodes (source and drain electrodes). The representative atomic force microscopy micrograph of the PAA electret films on SiO$_2$ revealed a smooth and uniform surface with a low root-mean-square (RMS) roughness value below 1 nm, as depicted in Figure S11. The pentacene semiconductor growing on this surface could crystallize well and suppress interface traps between the semiconductor and electret layers. In addition, the PAA films possess moderate hydrophobic behavior with a water contact angle of 83−87°, indicating that the characteristic of low surface energy could improve the wettability of pentacene on the smooth electret surface.[26−28] Consequently, all PAA

electrets could offer a beneficial environment to deposit well-growth pentacene.

Figure S12 presents the electrical hysteresis characteristics of pentacene-based OFETs with PAA electrets in an inert atmosphere at room temperature operated in forward (20 to −100 V) and backward (−100 to 20 V) scanning of gate voltage with a fixed source-to-drain voltage of −60 V. Generally, the behavior of hysteresis in the electrical characteristics of OFETMs is associated with the trapping of charge carriers in electret layers. Owing to the polarity of trapping charges, the internal electrical field could be constructed and possibly shield the electrical field from gate electric stress. On the other hand, the span of the dual-sweeping curves could not only elucidate the ability of charge storage but also deliver information on the polarity of trapping charge. First, the memory device with **PDTPmC** as an electret layer demonstrates a considerably huge hysteresis span in-between the forward and backward scanning, and the **PTTP**-based memory device exhibits a moderate effect. In contrast to the memory devices employing **PDTPmC** and **PTTP**, the **PTTC**-based memory device could hardly observe the hysteresis behavior. Accordingly, the **PDTPmC**-based memory device reveals the most outstanding hole-trapping ability.

To further explore the memory characteristics of pentacene-based PAA transistor memory devices, successive steps of gate pulses (V_G) were exerted on the memory devices for different charge trapping-density states, as shown in Figure 5. The electrical transfer characteristics of the fabricated pentacene-type PAAs memory devices display a typical p-type accumulation mode with good current modulation. All the measurements were conducted under a fixed source-to-drain voltage of −60 V and in the natural dark environment to exclude the light-induced charge transfer or excitons.[29] The transfer curves of PAAs-based transistor memory devices could be obtained by introducing gate biases from −20, −40, −60, −80, and −100 to −120 V for 1 s as a programming (writing) process. As the results illustrated in Figure 6a−c, the bias-induced transfer curves shift toward a more negative direction than the initial curve (black line) as significant negative pulses are applied. Namely, the electric-stress-induced hole channel in the semiconducting layer could be generated and injected into the charge storage layer. Therefore, the degree of shifting behavior solely depends on the design structures of the polymer electrets. The most shifted curve for the PDTPmC memory device under a −120 V electric stress for 1 s can be observed. For organic transistor memory, the memory window (MW) is an indicative and crucial parameter defined as the difference in threshold voltages between the initial and programming curves. In Figure S13, the MW of PAAs-based
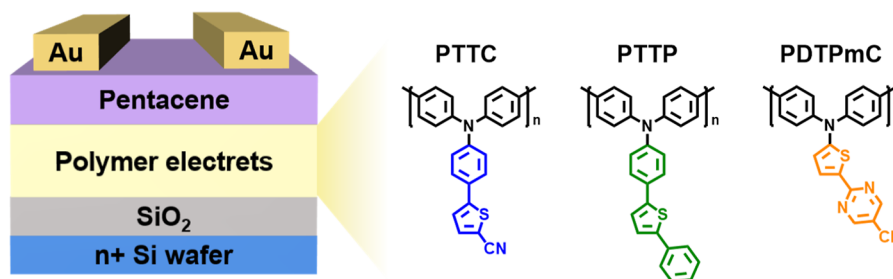

Figure 4. Schematic configuration of the pentacene-based PAA OFET memory device and the corresponding chemical structure of various polymer dielectrics.
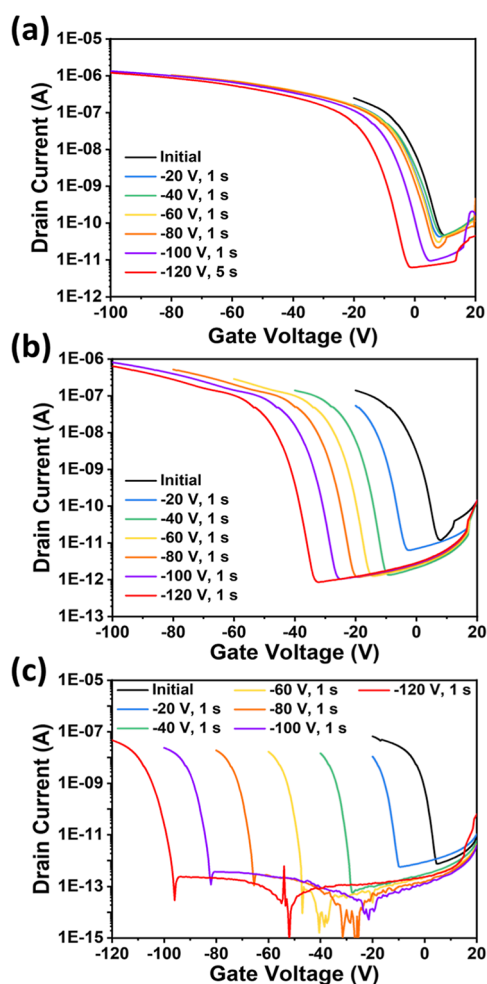
Figure 5. Memory characteristics of the (a) **PTTC**, (b) **PTTP**, and (c) **PDTPmC** memory devices operated by various negative applied gate pulses (from −20, −40, −60, −80 V, and −100 to −120 V for 1 s). All measurements were in the dark at a fixed drain voltage (V_{DS} = −60 V).

Figure 6. Sequential hysteresis curves of (a) **PTTC**, (b) **PTTP**, and (c) **PDTPmC** memory devices by dual sweeps from 20 to −100 V for initial, after electrical writing (−120 V, 1/5 s), and ERS (+120 V, 10 s) processes.

transistor memory devices manifest monotonically enlarging characteristics with the increase in the applied gate pulses, and the results are tabulated in Table S8.

The increased shifts in the transfer curve upon application of different programming voltage stresses demonstrate that the trapping density of holes that migrate from pentacene into the PAAs electrets is controllable. The memory windows are 13, 44, and 106 V for **PTTC**, **PTTP**, and **PDTPmC** memory devices, respectively. It is worth noting that polymeric electrets [PVN, PVTT, and P(St-Fl)₃] with conjugated structures demonstrate that tuning the energy level to align with semiconducting materials resulting in reducing the barrier between the charge storage and the semiconducting layers to facilitate the efficiency of charge transfer in previous reports.[8,24,36] Herein, PAAs electrets with a similar HOMO energy barrier allow hole transfer from the semiconductor to the polymer electret layers (as shown in Figure S14) However, the complete distinct storage ability of PAAs memory devices has been presented. Therefore, there is a lack of investigation to explain the relationship between polymer framework and charge storage behavior. First, the PTTP memory device exhibits a more significant charge storage capability than the PTTC memory device. The previously mentioned BLA
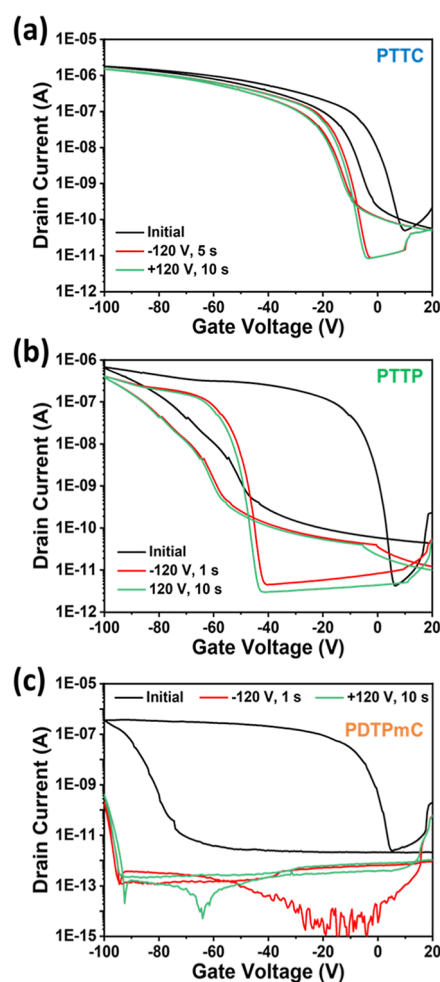
calculation results show that the polymer PTTP exhibits a more delocalized conjugated structure than PTTC. Namely, PTTP electret reveals hole vacancies for hole trapping and maintains charges. Consequently, the PTTP-based memory device demonstrates a better hole-trapping capability. Similarly, introducing a pi-extender can also improve the PTPA-CN electret's poor hole-trapping ability. Compared to the PTPA-CN,[19] the hole-trapping capability of the PTTC electret could be improved from an almost invisible 5 V (PTPA-CN as the electret) to 13 V as a thiophene spacer is introduced to the triphenylamine core. Second, PTTP and PDTPmC, both electrets, feature well-coplanar properties, especially for the DTPmC structure, as shown in Figure 1a. The result of memory characteristics implied that the PDTPmC memory device expresses an incredible hole-trapping performance compared to the PTTP memory device. In other words, other crucial factors affect charge storage behavior besides the alignment of energy level and coplanarity. Dielectric materials with a high dipole moment are frequently essential to discuss in thin-film transistors since the high concentration of charges has easily been induced and accumulated in the interface of the semiconducting and the dielectric layers.[37] The results in Figure S7 indicate that donor−acceptor fused DTPmC features more robust ICT (or intense dipole moment) than

TTP molecular. Hence, the excellent charge transfer characteristics within the molecular structure to facilitate the carrier density produced in the hole channel led to the PDTPmC-based memory device exhibiting a much more effective hole storage behavior. Nevertheless, PTTC and PDTPmC polymers possess similar HOMO energy levels and donor–acceptor frameworks, but the PTTC polymer lacks a planar structure to accumulate and retain charges. There is an entirely distinct hole-trapped capability for the PTTC and the PFTPmC memory device, 13 and 106 V, respectively. In short, the result indicates that the PDTPmC electret possessing a highly planar conformation and thus enhanced conjugated structure and ICT character provides a beneficial design strategy to demonstrate outstanding electrical-driven hole-trapping capability.

Additionally, the dual sweep loops for electrical programming and ERS operations of the PAA-based transistor memory devices are illustrated in Figure 6. The forward and backward transfer curves exhibit a similar trace after applying the negative bias, implying that the memory behavior of each polymer electret has achieved hole-storage saturation under an electrical stress of −120 V. Interestingly, all of the charged PAA-based memory devices could not return to the neutral state, maintaining the similar trace even upon an opposite polarity bias (gate bias of +120 V, 10 s). Since the trapped charge could be recombined with the reverse polarity charge from the semiconductor or released under opposite applied bias, the transistor memories exhibit reversible cyclic transfer characteristics with an apparent hysteresis upon their dual sweeps. However, the pentacene-base transistor memory devices incorporating PAAs electrets show an irreversible switching behavior (or electrically nonerasable behavior), demonstrating write-once-read-many (WORM) behaviors. This result confirms that the device could maintain the stored data for a long time after a specific pulse was applied and allow data to be recorded but not erased. Generally, there are two possible mechanisms to explain this electrically nonerasable behavior. One is the considerable barrier of LUMO energy level between semiconducting materials and polymeric electrets, resulting in the electron not being able to inject into the electret layer. Another one is the holes being trapped tightly according to the polymeric electret with a more conjugated structure to stabilize charges.[24,30,31] Notably, although the PDTPmC electret and pentacene have similar LUMO energy levels, the PDTPmC memory device exhibits electrically nonerasable behavior still. Hence, the PAAs-based memory devices can stabilize the trapped charge and improve the charge storage ability.

3.4. Memory Characteristics of Photorecoverable PAAs Transistor Memory Devices.
The photoinduced recovery approach has recently been utilized to erase an electrical WORM-type memory device.[18,19] Moreover, conjugated polymers possess excellent photosensitivity and charge delocalization, thus becoming potential candidates for optically driven memory devices. Further procedures conducted to investigate the memory behavior and photoinduced recovery characteristics of the pentacene-based PAAs transistor memories are depicted in Figure 7. After the initial scanning, a negative gate bias (−120 V, 1 s) was applied to the PAAs-based memory devices. The transfer curves of these three devices based on the PTTC, PTTP, and PDTPmC electrets reveal a noticeably shifted sequence of MWs, indicating that the electrically induced holes could be effectively captured into
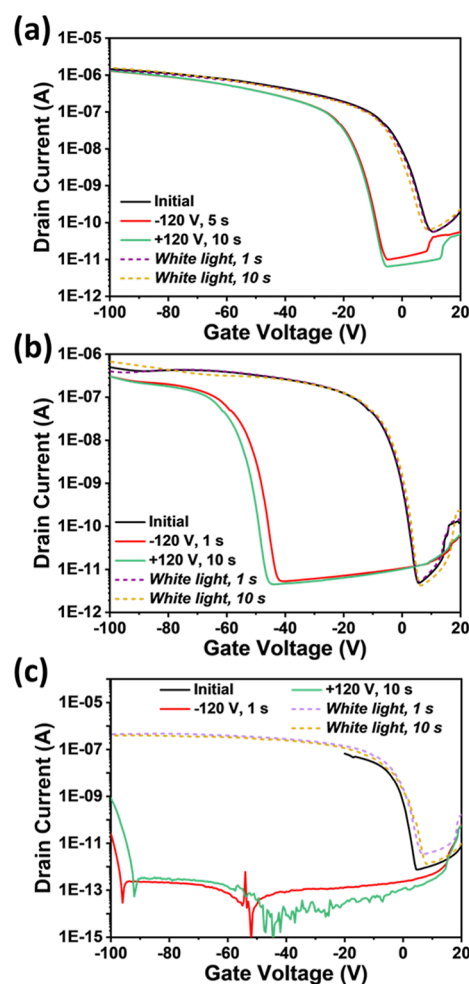

Figure 7. Pentacene-based transistor memory devices with (a) **PTTC**, (b) **PTTP**, and (c) **PDTPmC** as electrets operated in the procedures of electrical programming and optical-ERS, where optical operation irradiates white LED light with 25 mW cm^{-2}. All currents were measured in the dark at a fixed drain voltage ($V_{DS} = -60$ V).

the arylamine-based polymer electrets. Afterward, the positive gate bias with a longer operating time (+120 V, 10 s) was applied to the programmed PAAs memory devices for electrical ERS purposes. However, the corresponding transfer curves retain a trace similar to the programmed curves, indicating that the electrically induced electrons could not significantly inject into programmed electrets, resulting in the electrically unerasable features. The white light inhering characteristics of universality and convenience is the most commonly adopted as the source of photorecovery. All three PAAs memory devices were exposed to white LED light with the fixed light intensity (25 mW cm^{-2}) as illustrated dash line in Figure 7. The photoexcitation excitons could effectively be generated in the charged electret layer under light irradiation. Since the trapped charges could reduce the attractive force of photoexcited electron−hole pairs, the energy-enriched electrons are combined with trapped holes, serving as the behavior of photoinduced recovery. Therefore, the programmed PAAs memory devices could return to neutral under light exposure only for 1s. The whole working procedure of photoinduced recovery utilizing PAAs as electret is shown in Figure S15. Notably, the incredible number of stored charges in **PDTPmC** memory devices could reflect the fast photorecovery ability. In

Figure 7c, after exposing white light on the programmed **PDTPmC** memory device for 1 s, the resulting trace of the transfer curve is consistent with the original initial state, confirming that the photogenerated excitons could efficiently eliminate the captured holes at the programmed state because **PDTPmC** with the coplanar backbone could provide adequate delocalization ability for excitons to recombine the trapped charge.[32]

The light irradiation time has extended to PAAs-based memory devices from 1 to 10 s to investigate further the photoresponsive ability, as shown in Figure 7. Afterward, the longer irradiated time of the transfer curve exhibits an identical trace as the shorter irradiated time for all PAA-based memory devices. Namely, all the PAAs electrets show fast photo-recoverable ability for exposing 1 s to eliminate trapped charges. Furthermore, the PAAs-based memory devices possess light-ERS-only behavior.

In addition, the memory device featured the behavior of losing data, requiring periodic application of external voltage to maintain the storage message, serving as a more energy-consuming performance. The pentacene-based PAAs memory exhibits more energy-saving electrical programming behavior (WORM). It utilizes light illumination as another operation to recover the charged devices, called photoresponsive flash memory. The fast and effective photorecovery ability has been revealed in Figure 7. In addition, the electrical-programming process exhibited an energy-saving advantage, as presented in Figure S16. Owing to the high hole-affinity of the **PDTPmC** electret, the corresponding memory device demonstrates a larger memory window in the PAAs memory device under a fixed gate voltage of −30 V. Furthermore, the reading voltage set only at −5 V, the **PDTPmC** memory device also expresses the high current on−off ratio of approximately 10^5 between programmed and initial states. For the practical applications of memory devices, retention characteristics are an essential parameter, referring to the permanence of stored information. Long-term storage characteristics of the pentacene-based **PDTPmC** memory device are illustrated in Figure 8a. We measured the initial state of the **PDTPmC** memory device first, and then, a gate voltage of −30 V for 1 s was exerted in the memory device to create the low-current form. The programmed **PDTPmC** device could maintain a hole-trapping state for 10,000 s without significantly decreasing the drain current, indicating nonvolatile behavior. Sequentially, the programmed device could recover to the neutral state under white light for 1 s. The memory contrast ratio, a typical transistor memory parameter describing the difference in the current level, is 10^5 for the **PDTPmC** memory device.

Moreover, the cyclic switching measurement was conducted to evaluate the endurance of the **PDTPmC** photoresponsive memory device, as presented in Figure 8b,c. The procedure of four successive steps (write-read-erase-read, WRER) was designed to receive the drain current dependent on the modulated gate voltage, including electrical programmed (−30 V) for 1 s, reading step for 30 s, light irradiation for 1 s, and rereading for 30 s. All currents were recorded at −5 V, as shown in Figure S17. The 200 repeatable cycle measurements were successively achieved, which could meet the essential criteria of a photorecorder.

4. CONCLUSIONS

In conclusion, we successfully fabricated photoresponsive flash transistor memory constructed with oxidative polymerized
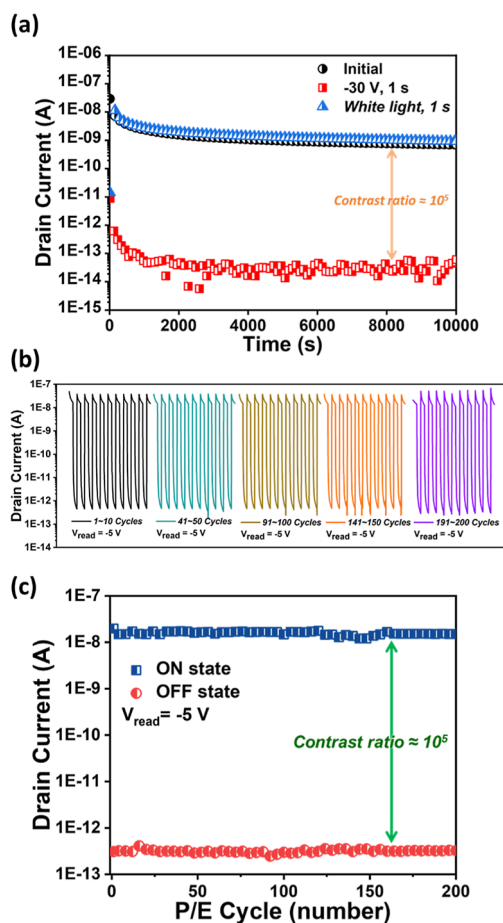

Figure 8. (a) Retention characteristics and contrast ratio after electric writing (V_G = −30 V) and light recovery operation (reading voltage: −5 V). (b) The expansion for 1−10, 41−50, 91−100, 141−150, and 191−200 cycles. The cycle time of the switching test was 62 s/cycle, including 1 s electrically programmed (V_G = −30 V), 30 s reading, 1 s white light illumination (25 mW cm^{-2}), and 30 s rereading; all currents were recorded at −5 V. (c) 200 switching cycles durability test for photorecorder application of the pentacene-based **PDTPmC** OFET memory devices.

polymers, PAA series, as a charge storage layer. Different pendant moieties in these conjugated polymer electrets for transistor memory have been investigated. Among them, the **PDTPmC** electret with a more planar donor−acceptor structure demonstrates excellent hole-trapping and photo-recovery capabilities. Owing to the high dipole moment of **PDTPmC** electret, the massive positive carrier channel under electrical stress could be more easily induced in the interface between the pentacene semiconductor and memory materials. Therefore, the electrical-induced hole would be trapped in the **PDTPmC** electret and storage would be stably caused by the approximate HOMO energy level and highly coplanar structure. From the viewpoint of photonic transistor memory, the coplanar and donor−acceptor structural design is beneficial for the photoexcitation excitons to separate into free charges and eliminate the stored information.

Furthermore, the memory device based on **PDTPmC** electret reveals nonvolatile characteristics at the programmed state and could maintain over 10^4 s with a high On/Off current ratio of 10^5. The electrical-programming and optical-ERS switchable test reveals stability and good durability over 200 continuous operating cycles for practical application as

electronic storage devices. A conceptual idea to design photoresponsive polyarylamine-based conjugated polymer is reported to lead to the outstanding performance of conventional transistor memory and photorecorder devices.

ASSOCIATED CONTENT

ⓈⒾ Supporting Information

The Supporting Information is available free of charge at https://pubs.acs.org/doi/10.1021/acsapm.3c01327.

> Synthetic route and chemical structure characterization for arylamine-based monomers and polymers (^{1}H NMR, FTIR, single crystal, cyclic voltammograms, and energy level); surface morphology of polymer and semiconducting materials deposited on the electret; and electric characteristics of polyarylamine-based conjugated polymer memory devices (PDF)

AUTHOR INFORMATION

Corresponding Authors

Guey-Sheng Liou − *Institute of Polymer Science and Engineering, National Taiwan University, Taipei 10617, Taiwan;* ⓞ orcid.org/0000-0003-3725-3768; Email: gsliou@ntu.edu.tw

Ken-Tsung Wong − *Department of Chemistry, National Taiwan University, Taipei 10617, Taiwan; Institute of Atomic and Molecular Science, Academia Sinica, Taipei 10617, Taiwan;* ⓞ orcid.org/0000-0002-1680-6186; Email: kenwong@ntu.edu.tw

Authors

Bo-Yuan Chuang − *Department of Chemistry, National Taiwan University, Taipei 10617, Taiwan*

Chun-Yao Ke − *Institute of Polymer Science and Engineering, National Taiwan University, Taipei 10617, Taiwan*

Yu-Jen Shao − *Institute of Polymer Science and Engineering, National Taiwan University, Taipei 10617, Taiwan*

Complete contact information is available at:
https://pubs.acs.org/10.1021/acsapm.3c01327

Author Contributions

‖B.Y.C., C.Y.K., and Y.J.S. contributed equally.

Notes

The authors declare no competing financial interest.
The crystallographic coordinates for the molecular structures in this study have been deposited at the Cambridge Crystallographic Data Centre (CCDC) under deposition numbers 2245696, 2245695, and 2245694 for the monomers of **TTP**, **TTC**, and **DTPmC**, respectively. The crystallographic data for **TTP**, **TTC**, and **DTPmC** are also available in the Supporting Information (Tables S9−S20).

ACKNOWLEDGMENTS

REFERENCES

(1) Li, Y.; Qian, Q.; Zhu, X.; Li, Y.; Zhang, M.; Li, J.; Ma, C.; Li, H.; Lu, J.; Zhang, Q. Recent Advances in Organic-Based Materials for Resistive Memory Applications. *InfoMat* **2020**, *2*, 995−1033.

(2) Chen, H.; Zhang, W.; Li, M.; He, G.; Guo, X. Interface Engineering in Organic Field-Effect Transistors: Principles, Applications, and Perspectives. *Chem. Rev.* **2020**, *120*, 2879−2949.

(3) Han, S. T.; Zhou, Y.; Roy, V. Towards the Development of Flexible Non-Volatile Memories. *Adv. Mater.* **2013**, *25*, 5425−5449.

(4) Kang, S. J.; Park, Y. J.; Bae, I.; Kim, K. J.; Kim, H. C.; Bauer, S.; Thomas, E. L.; Park, C. Printable Ferroelectric PVDF/PMMA Blend Films with Ultralow Roughness for Low Voltage Non-Volatile Polymer Memory. *Adv. Funct. Mater.* **2009**, *19*, 2812−2818.

(5) Baeg, K. J.; Noh, Y. Y.; Sirringhaus, H.; Kim, D. Y. Controllable Shifts in Threshold Voltage of Top-Gate Polymer Field-Effect Transistors for Applications in Organic Nano Floating Gate Memory. *Adv. Funct. Mater.* **2010**, *20*, 224−230.

(6) Baeg, K. J.; Noh, Y. Y.; Ghim, J.; Kang, S. J.; Lee, H.; Kim, D. Y. Organic Non-Volatile Memory Based on Pentacene Field-Effect Transistors Using a Polymeric Gate Electret. *Adv. Mater.* **2006**, *18*, 3179−3183.

(7) Chou, Y. H.; Chang, H. C.; Liu, C. L.; Chen, W. C. Polymeric Charge Storage Electrets for Non-Volatile Organic Field Effect Transistor Memory Devices. *Polym. Chem.* **2015**, *6*, 341−352.

(8) Hsu, J. C.; Lee, W. Y.; Wu, H. C.; Sugiyama, K.; Hirao, A.; Chen, W. C. Non-volatile Memory Based on Pentacene Organic Field-Effect Transistors with Polystyrenepara-Substituted Oligofluorene Pendent Moieties as Polymer Electrets. *J. Mater. Chem.* **2012**, *22*, 5820−5827.

(9) Park, H. L.; Kim, H.; Lim, D.; Zhou, H.; Kim, Y. H.; Lee, Y.; Park, S.; Lee, T. W. Retina-Inspired Carbon Nitride-Based Photonic Synapses for Selective Detection of UV Light. *Adv. Mater.* **2020**, *32*, 1906899.

(10) Jeong, Y. J.; Yun, D. J.; Kim, S. H.; Jang, J.; Park, C. E. Photoinduced Recovery of Organic Transistor Memories with Photoactive Floating-Gate Interlayers. *ACS Appl. Mater. Interfaces* **2017**, *9* (13), 11759−11769.

(11) Ke, C. Y.; Chen, M. N.; Chen, M. H.; Li, Y. T.; Chiu, Y. C.; Liou, G. S. Novel Authentic and Ultrafast Organic Photorecorders Enhanced by AIE-Active Polymer Electrets via Interlayer Charge Recombination. *Adv. Funct. Mater.* **2021**, *31*, 2101288.

(12) Ke, C. Y.; Chen, M. H.; Liou, G. S. High-Performance Aggregation-Induced Emission Active Poly(ether sulfone)s as Polymeric Electret for Energy-Saving Genuine Photonic Transistor Memory. *Chem. Eng. J.* **2023**, *457*, 141209.

(13) Ahmed, T.; Tahir, M.; Low, M. X.; Ren, Y.; Tawfik, S. A.; Mayes, E. L. H.; Kuriakose, S.; Nawaz, S.; Spencer, M. J. S.; Chen, H.; Bhaskaran, M.; Sriram, S.; Walia, S. Fully Light-Controlled Memory and Neuromorphic Computation in Layered Black Phosphorus. *Adv. Mater.* **2021**, *33*, 2004207.

(14) Chen, C. H.; Wang, Y.; Michinobu, T.; Chang, S. W.; Chiu, Y. C.; Ke, C. Y.; Liou, G. S. Donor-Acceptor Effect of Carbazole-Based Conjugated Polymer Electrets on Photo-responsive Flash Organic Field-Effect Transistor Memories. *ACS Appl. Mater. Interfaces* **2020**, *12*, 6144−6150.

(15) Yang, Y. F.; Chiang, Y. C.; Lin, Y. C.; Li, G. S.; Hung, C. C.; Chen, W. C. Highly Efficient Photoinduced Recovery Conferred Using Charge-Transfer Supramolecular Electrets in Bistable Photonic Transistor Memory. *Adv. Funct. Mater.* **2021**, *31*, 210217.

(16) Cheng, S. W.; Han, T.; Huang, T. Y.; Chang Chien, Y. H.; Liu, C. L.; Tang, B. Z.; Liou, G. S. Novel Organic Phototransistor-Based Non-volatile Memory Integrated with UV-Sensing/Green-Emissive Aggregation Enhanced Emission (AEE)-Active Aromatic Polyamide Electret Layer. *ACS Appl. Mater. Interfaces* **2018**, *10*, 18281−18288.

(17) Prakoso, S. P.; Li, Y. T.; Lai, J. Y.; Chiu, Y. C. Concept of Photoactive Invisible Inks toward Ultralow-Cost Fabrication of Transistor Photomemories. *Adv. Electron. Mater.* **2023**, *9*, 2201147.

(18) Chen, C. H.; Wang, Y.; Tatsumi, H.; Michinobu, T.; Chang, S. W.; Chiu, Y. C.; Liou, G. S. Novel Photoinduced Recovery of OFET

Memories Based on Ambipolar Polymer Electret for Photorecorder Application. *Adv. Funct. Mater.* **2019**, *29*, 1902991.

(19) Ke, C. Y.; Chen, M. N.; Chiu, Y. C.; Liou, G. S. Luminescence Behavior and Acceptor Effects of Ambipolar Polymeric Electret on Photorecoverable Organic Field-Effect Transistor Memory. *Adv. Electron. Mater.* **2021**, *7*, 2001076.

(20) Leliège, A.; Blanchard, P.; Rousseau, T.; Roncali, J. Triphenyl-amine/Tetracyanobutadiene-Based D–A–D π-Conjugated Systems as Molecular Donors for Organic Solar Cells. *Org. Lett.* **2011**, *13* (12), 3098–3101.

(21) Lin, L. Y.; Tsai, C. H.; Wong, K. T.; Huang, T. W.; Wu, C. C.; Chou, S. H.; Lin, F.; Chen, S. H.; Tsai, A. I. Efficient Organic DSSC Sensitizers Bearing An Electron-Deficient Pyrimidine as An Effective π-Spacer. *J. Mater. Chem.* **2011**, *21*, 5950–5958.

(22) Chiu, S. W.; Lin, L. Y.; Lin, H. W.; Chen, Y. H.; Huang, Z. Y.; Lin, Y. T.; Lin, F.; Liu, Y. H.; Wong, K. T. A Donor-Acceptor-Acceptor Molecule for Vacuum-Processed Organic Solar Cells with A Power Conversion Efficiency of 6.4%. *Chem. Commun.* **2012**, *48*, 1857–1859.

(23) Geng, X.; Li, D.; Tang, K.; Wang, G.; Miao, Y.; Guo, K. π-Bridge Dependent Efficient Aggregation-Induced Emission Character-istic and Significant Mechanofluorochromic Behavior. *J. Lumin.* **2022**, *248*, 118925.

(24) Baeg, K. J.; Noh, Y. Y.; Ghim, J.; Lim, B.; Kim, D. Y. Polarity Effects of Polymer Gate Electrets on Non-Volatile Organic Field-Effect Transistor Memory. *Adv. Funct. Mater.* **2008**, *18*, 3678–3685.

(25) Chou, Y. H.; You, N. H.; Kurosawa, T.; Lee, W. Y.; Higashihara, T.; Ueda, M.; Chen, W. C. Thiophene and Selenophene Donor-Acceptor Polyimides as Polymer Electrets for Non-volatile Transistor Memory Devices. *Macromolecules* **2012**, *45* (17), 6946–6956.

(26) Fritz, S. E.; Kelley, T. W.; Frisbie, C. D. Effect of Dielectric Roughness on Performance of Pentacene TFTs and Restoration of Performance with A Polymeric Smoothing Layer. *J. Phys. Chem. B* **2005**, *109*, 10574–10577.

(27) Ruiz, R.; Choudhary, D.; Nickel, B.; Toccoli, T.; Chang, K. C.; Mayer, A. C.; Clancy, P.; Blakely, J. M.; Headrick, R. L.; Iannotta, S.; Malliaras, G. G. Pentacene Thin Film Growth. *Chem. Mater.* **2004**, *16*, 4497–4508.

(28) Jang, M.; Lee, M.; Shin, H.; Ahn, J.; Pei, M.; Youk, J. H.; Yang, H. Balancing Surface Hydrophobicity and Polarizability of Fluorinated Dielectrics for Organic Field-Effect Transistors with Excellent Gate-Bias Stability and Mobility. *Adv. Mater. Interfaces* **2016**, *3*, 1600284.

(29) Guo, Y.; Di, C. A.; Ye, S.; Sun, X.; Zheng, J.; Wen, Y.; Wu, W.; Yu, G.; Liu, Y. Multibit Storage of Organic Thin-Film Field-Effect Transistors. *Adv. Mater.* **2009**, *21*, 1954–1959.

(30) Chiu, Y. C.; Liu, C. L.; Lee, W. Y.; Chen, Y.; Kakuchi, T.; Chen, W. C. Multilevel Non-volatile Transistor Memories Using A Star-Shaped Poly((4-diphenylamino)benzyl methacrylate) Gate electret. *NPG Asia Mater.* **2013**, *5*, No. e35.

(31) Chiu, Y. C.; Sun, H. S.; Lee, W. Y.; Halila, S.; Borsali, R.; Chen, W. C. Oligosaccharide Carbohydrate Dielectrics toward High-Performance Non-volatile Transistor Memory Devices. *Adv. Mater.* **2015**, *27*, 6257–6264.

(32) Park, K. H.; Kim, W.; Yang, J.; Kim, D. Excited-State Structural Relaxation and Exciton Delocalization Dynamics in Linear and Cyclic π-Conjugated Oligothiophenes. *Chem. Soc. Rev.* **2018**, *47*, 4279–4294.

(33) Kumari, B.; Paramasivam, M.; Mukherjee, T.; Khandelwal, S.; Dutta, A.; Kanvah, S. A competitive effect of acceptor substitutions on the opto-electronic features of triphenylamine cored di α-cyanostilbene derivatives. *New J. Chem.* **2021**, *45*, 4683–4693.

(34) Huang, Z.; Tang, F.; He, F.; Kong, L.; Huang, J.; Yang, J.; Ding, A. Pyrene and Triphenylamine Substituted Cyanostyrene and Cyanostilbene Derivatives with Dual-State Emission for High-Contrast Mechanofluorochromism and Cell Imaging. *Org. Chem. Front.* **2022**, *9*, 5118–5124.

(35) Guo, S.; Pan, J.; Huang, J.; Kong, L.; Yang, J. Two AIEE-active α-cyanostilbene derivatives containing BF$_2$ unit for detecting explosive picric acid in aqueous medium. *RSC Adv.* **2019**, *9*, 26043–26050.

(36) Chou, Y. H.; Takasugi, S.; Goseki, R.; Ishizone, T.; Chen, W. C. Nonvolatile Organic Field-Effect Transistor Memory Devices Using Polymer Electrets with Different Thiophene Chain Lengths. *Polym. Chem.* **2014**, *5*, 1063–1071.

(37) Wu, W.; Zhang, H.; Wang, Y.; Ye, S.; Guo, Y.; Di, C.; Yu, G.; Zhu, D.; Liu, Y. High-Performance Organic Transistor Memory Elements with Steep Flanks of Hysteresis. *Adv. Funct. Mater.* **2008**, *18*, 2593–2601.

🕮 Recommended by ACS